Published in final edited form as:

Reproduction. 2022 August 01; 164(2): 41–54. doi:10.1530/REP-22-0123.

Early growth response 1 transcription factor is essential for the pathogenic properties of human endometriotic epithelial cells

Vineet K. Maurya[1], **Maria M. Szwarc**[1], **Rodrigo Fernandez-Valdivia**[2], **David M. Lonard**[1], **Yong Song**[4], **Niraj Joshi**[4], **Asgerally T. Fazleabas**[4], **John P. Lydon**[1,*]

[1]Department of Molecular and Cellular Biology, Baylor College of Medicine, Houston, Texas, USA

[2]Department of Pathology, Wayne State University School of Medicine, Detroit, Michigan, USA

[4]Department of Obstetrics, Gynecology & Reproductive Biology, Michigan State University, Grand Rapids, Michigan

Abstract

Although a non-malignant gynecological disorder, endometriosis displays some pathogenic features of malignancy, such as cell proliferation, migration, invasion and adaptation to hypoxia. Current treatments of endometriosis include pharmacotherapy and/or surgery, which are of limited efficacy and often associated with adverse side-effects. Therefore, to develop more effective therapies to treat this disease, a broader understanding of the underlying molecular mechanisms that underpin endometriosis needs to be attained. Using immortalized human endometriotic epithelial and stromal cell lines, we demonstrate that the early growth response 1 (EGR1) transcription factor is essential for cell proliferation, migration and invasion, which represent some of the pathogenic properties of endometriotic cells. Genome-wide transcriptomics identified an EGR1-dependent transcriptome in human endometriotic epithelial cells that potentially encodes a diverse spectrum of proteins that are known to be involved in tissue pathologies. To underscore the utility of this transcriptomic dataset, we demonstrate that carbonic anhydrase IX (CAIX), a homeostatic regulator of intracellular pH, is not only a molecular target of EGR1 but is important for maintaining many of the cellular properties of human endometriotic epithelial cells that are also ascribed to EGR1. Considering therapeutic intervention strategies are actively being developed for EGR1 and CAIX in the treatment of other pathologies, we believe EGR1 and its transcriptome (which includes CAIX) will offer not only a new conceptual framework to advance our understanding of endometriosis but will furnish new molecular vulnerabilities to be leveraged as potential therapeutic options in the future treatment of endometriosis.

*Correspondence should be addressed to JP Lydon; jlydon@bcm.edu.

Author contribution statement

VKM, MMS, DML, and JPL designed and/or executed the experiments in the manuscript. RF performed part of the bioinformatics analyses. YS, NJ and ATF contributed to the non-human primate endometriosis immunohistochemical studies as well as generating and providing the iEc-ESC line. The studies were supervised by JPL, and most of the manuscript and figures were prepared by VKM, MMS, DML and JPL. All authors read and approved the final manuscript.

Supplementary materials

This is the link to the online version of the paper at XYZ.

Declaration of interest

The authors declare that no conflict of interest could be perceived as prejudicing the impartiality of the research reported.

Keywords

Early growth response 1; human; baboon; endometriosis; epithelial; proliferation; migration; invasion; RNA-seq; carbonic anhydrase IX

Introduction

Early growth response 1 (EGR1; also known as NGFI-A, Zif 268 or Krox 24) is a member of the EGR family of Cys_2-His_2-type zinc finger transcription factors that also includes EGR2, EGR3 and EGR4 (Gashler and Sukhatme, 1995, O'Donovan et al., 1999, Sukhatme, 1990). In response to a broad spectrum of extracellular stimuli, EGR family members mediate transcriptional responses through direct interaction of their three tandem DNA binding motifs with a GC-rich consensus sequence (GCG(T/G)GGGCG) within regulatory regions of target genes (Benos et al., 2002, Swirnoff and Milbrandt, 1995). Through these target genes, EGR1 controls a myriad of cellular properties from proliferation, differentiation, migration, invasion to programmed cell death and stemness (Gururajan et al., 2008, Ma et al., 2021, Madden and Rauscher, 1993, Yan et al., 2021, Yan et al., 2000, Zhang et al., 2021, Zhao et al., 2021). Such cellular responses drive EGR1's Early investigations in the mouse demonstrated that EGR1 ablation results in a block in the expression of the luteinizing hormones.

Early investigations in the mouse demonstrated that EGR1 ablation results in a block in the expression of the luteinizing hormone β-subunit in the pituitary gonadotrope, resulting in impaired ovulation and luteinization (Lee et al., 1996, Topilko et al., 1998, Wolfe and Call, 1999). In the uterus, studies revealed that *Egr1* transcript levels are rapidly induced by estrogen in the epithelial and stromal cellular compartments of the murine endometrium during early pregnancy (Guo et al., 2014, Kim et al., 2014, Kim et al., 2018, Liang et al., 2014). These studies also indicated that endometrial EGR1 expression in the luminal epithelium and pre-decidual stromal cells is required for embryo implantation and subsequent decidualization (Guo et al., 2014, Kim et al., 2014, Kim et al., 2018, Liang et al., 2014). Recent investigations on human endometrial stromal cells in culture support the findings in the mouse as well as a role for EGR1 in priming the pre-decidual stromal cell for decidualization when exposed to a deciduogenic hormone stimulus (Kommagani et al., 2016, Szwarc et al., 2019).

Apart from its function in normal physiological processes, EGR1 plays important roles in the pathogenesis of numerous target tissues (Wang et al., 2021a, Hao et al., 2021). Therefore, we asked whether EGR1 is involved in the pathology of the uterus in addition to its established role in normal uterine functions. Here, we demonstrate that EGR1 is critical for the pathogenic properties of human endometriotic epithelial and stromal cells, which include cellular proliferation, migration and invasion. Moreover, genome-wide transcriptome analysis highlights distinct gene expression programs that mediate EGR1's contribution to the pathogenic properties of human endometriotic epithelial cells, which encompass cytokine signaling, adaptation to hypoxia, cellular inflammatory responses, epithelial-mesenchymal transition, and cell-cell communication. To underscore the utility

of the EGR1 transcriptome dataset, we observed carbonic anhydrase IX (CAIX) is a critical EGR1 responsive molecular target that drives many of the pathogenic properties of the human endometriotic epithelial cell.

Materials and methods

Immunohistochemical analysis of baboon (Papio anubis) endometriotic tissue

Eutopic uterine tissue and matched ectopic endometriotic lesions (at pelvic and peritoneal locations) were obtained from a baboon model for endometriosis (n=4). As previously described (D'Hooghe et al., 1994, Fazleabas, 2006b, Fazleabas et al., 2002), the baboon model for endometriosis entails autologous inoculation of menstrual endometrium into the peritoneal cavity, modeling retrograde menstruation. Eutopic and ectopic tissues were collected during the mid-secretory phase of the cycle (days: 9-12 postovulation), 15 months following disease induction. Importantly, endometriotic lesions derived from the baboon endometriosis model share morphological and histological characteristics similar to those observed in human lesions (Fazleabas et al., 2002). At the time of harvesting these tissues, all animal procedures used for the experimental induction of endometriosis in the baboon were prospectively approved by the Institutional Animal Care and Use Committee (IACUC) at the University of Illinois, Chicago Michigan State University.

For immunohistochemical analyses, tissues were fixed overnight in 4% paraformaldehyde in phosphate-buffered saline (PBS) before paraffin embedding and sectioning onto slides. Immunohistochemical detection of EGR1 and CAIX was achieved using primary rabbit monoclonal antibodies (anti-EGR1 (#4153) and anti-CAIX (#5649); Cell Signaling Technology Inc., Danvers, MA; each diluted 1:100) followed by incubation with a horseradish peroxidase (HRP)-conjugated goat anti-rabbit secondary antibody (Vector Laboratories, Burlingame CA (P-1000); diluted 1:200). Peroxidase activity was detected with the Vectastain Elite ABC-HRP kit (Vector Laboratories Inc., Burlingame, CA). Following immunostaining, tissue sections were counterstained with hematoxylin before applying Permount mounting medium to affix coverslips.

Immortalized human endometriotic cell lines

The immortalized human endometriotic epithelial cell (iHEEC/Luc (referred to as iHEEC hereon) line has been described (Bono et al., 2012, Han et al., 2012). Briefly, the iHEEC line (formerly known as EMOSIS-CC/TERT1 (Bono et al., 2012)) was derived from a human ovarian endometrioma and immortalized by transfection with the human telomerase reverse transcriptase (hTERT) gene and subsequently modified with a luciferase reporter using lentivirus (Bono et al., 2012, Han et al., 2012). The iHEEC line was cultured in DMEM/F12 medium supplemented with 10% fetal bovine serum (FBS; Sigma-Aldrich, St. Louis, MO) and a 1% penicillin-streptomycin antibiotic solution (ThermoFisher Scientific Inc. Waltham, MA); medium was changed every other day. Using the American Type Culture Collection (ATCC) cell line authentication service, the iHEEC line was authenticated by short tandem repeat (STR) profiling analysis. The immortalized human endometriotic stromal cell line (iEc-ESC) and its culture have been described previously (Song et al., 2020a).

Transfection of small interfering RNAs

Human endometriotic cells were cultured in six-well plates in triplicate before transfection with sixty picomoles of the non-targeting (*NT*) siRNA ((D-001810-10-05) Dharmacon Inc., Lafayette, CO), or siRNAs targeting either *EGR1* ((L-006526-00-0005) Dharmacon Inc.) or *CAIX* ((L-005244-00-00005) Dharmacon Inc.) using the Lipofectamine RNAiMAX transfection reagent (Invitrogen Corporation, Carlsbad, USA) (Szwarc et al., 2019). Forty-eight hours post-transfection, cells were harvested for quantitative real-time (qRT) PCR, RNA-seq, or western immunoblot analysis. Alternatively, cells were trypsinized and re-plated to assay for cell proliferation/viability, clonogenic survival or invasion capabilities (Cagle et al., 2019, Szwarc et al., 2018a, Zhang et al., 2018).

Quantitative real-time PCR

Cells were lysed in RNA lysis buffer before total RNA was isolated with the Purelink RNA Mini Kit ((#12183020) ThermoFisher Scientific Inc.). The Nano-Drop 2000 UV/Visual spectrophometer (ThermoFisher Scientific Inc.) was used for RNA quantification; RNA (1 μg) was reverse transcribed using the High-Capacity cDNA Reverse Transcription Kit ((#4368814) ThermoFisher Scientific Inc.). Amplified cDNA was diluted to 10 ng/μl before qRT-PCR was performed using the Fast TaqMan 2X Mastermix (Applied Biosystems/Life Technologies, Grand Island, NY). The TaqMan assays used in this study are listed in Table 1. All qRT-PCR experiments were performed using the 7500 Fast Real-time PCR system (Applied Biosystems/Life Technologies, Grand Island, NY); the delta-delta cycle threshold was used to normalize expression to the 18S reference.

Global RNA expression profiling

Genome-wide RNA-sequencing (RNA-seq) and analysis were performed as previously described (Szwarc et al., 2019, Szwarc et al., 2018b). Briefly, total RNA purity and integrity were assessed using the NanoDrop spectrophotometer (ThermoFisher Scientific Inc.), and the 2100 Bioanalyzer with RNA chips (Agilent Technologies, Santa Clara, CA) respectively. Only RNA samples scoring a RNA integrity number (RIN) of 8 or greater were included. For each experimental group, RNA samples from three replicates were used. Sequencing libraries were prepared using the TruSeq Stranded mRNA kit (Illumina Inc., San Diego, CA) from 250 ng of RNA and PCR amplified. Quality analysis of resultant libraries was performed on the 4200 TapeStation with D1000 ScreenTape assays (Illumina Inc.). Adapter-ligated fragment concentration was estimated by qRT-PCR assay with a KAPA Library Quantification Kit (KAPA Biosystems, Wilmington, MA). After equimolar pooling, libraries were quantified on the 2100 Bioanalyzer (using the High Sensitivity DNA Kit and DNA chips) and the KAPA Library Quantification Kit. Sequencing of libraries was performed on the NovaSeq platform (Ilumina Inc.). Paired-end 100 base pair (bp) sequencing reads were generated at mid-output and mapped to the human genome. Raw sequenced reads in Ilumina fastq file format were aligned to the human genome (Genome Reference Consortium Human Build hg38 (National Center for Biotechnology Information (NCBI))) through use of the ultrafast universal RNA-seq aligner: spliced transcripts alignment to a reference (STAR) (Dobin et al., 2013, Anders et al., 2015). The number of reads aligned to known genes was determined by the Python-based software package HTSeq (Anders et al., 2015) (http://

www-huber.embl,de/users/anders/HTSeq). To reduce possible PCR bias, read duplicates were removed with Picard Tools (http://broad.institute.github.10/picard).

The Bioconductor package EdgeR was applied to the gene expression data to detect differentially expressed genes between the two groups (Robinson et al., 2010). The false discovery rate (FDR) of differentially expressed genes was estimated using the Benjamini and Hochberg method (Benjamini, 1995). Gene expression comparisons with an FDR ≤ 0.05 and an absolute fold change (IFCI) ≥ 1.5 were considered to be significantly differentially expressed between the two groups. Genes with significantly altered expression (IFCI ≥ 1.5; FDR ≤ 0.05) between the two groups were used further to identify affected pathways (Huang da et al., 2009). Fragments per kilobase of transcript per million (FPKM) values of transcripts were used for hierarchical clustering; the pheatmap package in R was used to draw the clustered heatmap. Using raw gene count data, principal component analysis (PCA) was performed with the R function prcomp package (https://cran.r-project.org). All raw data files were deposited in Gene Expression Omnibus repository at the NCBI ((GSE199526) www.ncbi.nlm.gov/geo). Gene ontology enrichment analysis was performed using the DAVID (Database for Annotation, Visualization, and Integrated Discovery) functional annotation clustering tool (http://david.abcc.ncifcrff.gov/) (Sherman et al., 2007). Established gene sets overrepresented in our RNA-seq datasets were identified by Gene Set Enrichment Analysis (GSEA; http://software.broadinstitute.org/gsea/) (Mootha et al., 2003, Subramanian et al., 2005). Hallmark gene sets from the Molecular Signatures Database (MSigDB) were used in these GSEA studies (Liberzon et al., 2011).

Immunoblotting

Protein (20 μg) from cell lysates was resolved on 4-15% sodium dodecyl sulfate-polyacrylamide (SDS-PAGE) gels before transfer to polyvinylidene difluoride (PVDF) membranes. Following protein transfer, PVDF membranes were blocked for 1 hour with 5% non-fat dry milk ((sc-2324 (Blotto)) Santa Cruz Biotechnology Inc., Dallas, Texas) in Tris-buffered saline with Tween 20 (TBS-T) and incubated overnight at 4°C with the following primary antibodies: anti-EGR1 (#4154, Cell Signaling Technology, Inc., Danvers, MA) diluted 1:1000 and anti-β-actin (#A00702, GenScript Biotech, Piscataway, NJ) diluted 1:100000 in 5% non-fat milk in TBS-T. Blots were then probed with anti-rabbit ((A27036 (1:5000 dilution)) ThermoFisher Scientific Inc.) and anti-mouse IgG secondary antibodies conjugated with HRP ((#7076 (1:10000 dilution)) Cell Signaling Technology, Inc.) respectively in 5% non-fat milk in TBS-T for 1 hour at room temperature. Chemiluminescence was detected with the SuperSignal West Pico PLUS Chemiluminescent Substrate ((#1863097) ThermoFisher Scientific, Inc.). Immunoreactive bands were digitally imaged using the Bio-Rad ChemiDoc imaging system (Bio-Rad Laboratories, Hercules, CA).

Cell proliferation/viability assay

Cells were seeded in 96-well culture plates in triplicate, at a density of $5x10^3$ cells per well. Cells transfected with siRNAs for 48 hours were further cultured for 0, 24, 48, 72 or 96 hours before cell proliferation was measured using the CellTiter 96® Non-Radioactive Cell Proliferation Assay kit ((#G4000) Promega Inc. Madison, WI). After a specific time period

in culture, 15μl of 3-(4, 5-dimethylthiazol-2-yl)-2, 5-diphenyltetrazolium bromide (MTT); Promega, Madison, WI) was added to each well to a final concentration of 0.5mg/ml. Cells were then incubated at 37°C for an additional three hours in the dark. Following the three-hour incubation period, the supernatant was removed. Formazan crystals within wells were dissolved by the addition of the stop/solubilizing solution (100 μl (dimethyl sulfoxide (DMSO)/well)) before a further incubation period of 15 minutes at 37°C with gentle agitation. The absorbance of the final mixture was recorded at 570 nm (formazan absorbance maximum (Campling et al., 1988, Mosmann, 1983)) using a 96 well microplate ELISA reader. Relative cell proliferation was calculated as: mean absorbance at "N" time point/mean absorbance at 0 hour (h); N= 0, 24, 48, 72, and 96h. Each experiment was repeated three times with three to five technical replicates for each treatment group.

Clonogenic survival assay

Forty-eight hours post siRNA transfection, cells were cultured in six-well culture plates ($3x10^3$ cells per well in triplicate). Cells were incubated for ten days; medium was replaced every other day. After the ten-day culture period, cells were fixed with 4% paraformaldehyde for 15 minutes, washed with PBS for 10 minutes before colonies were stained with crystal violet solution (0.5%) for 15 minutes (Kommagani et al., 2013). After the sequential steps of de-staining in tap water and air-drying, stained colonies were photographed and counted. Each experiment was repeated three times with triplicates for each treatment group.

Cell migration assay

Cell migration was assessed using the *in vitro* wound-healing assay (Grada et al., 2017, Todaro et al., 1965). Briefly, cells were seeded in six-well culture plates and cultured until reaching 70–80% confluency before siRNA transfection. Using a 200-μl sterile pipette tip, a linear scratch (wound) was created in the middle of the cell monolayer within each well. Wells were gently washed to remove detached cells before image capture with an inverted phase-contrast microscope (EVOS™ XL Core Imaging System, #AMEX1000 (ThermoFisher Scientific Inc.)). Cells were incubated for forty-eight hours before the degree of wound closure was recorded by digital image capture. The wound area was calculated by manual tracing the cell-free area within captured images using ImageJ software (https://imagej.nih.gov/ij/). Results were expressed as a percent of wound closure in comparison to control after a forty-eight hours culture period (percent cell migration area = wound width at 0 h – wound width at 48 h/wound width at 0 h). Each experiment was repeated three times with triplicates for each treatment group.

Transwell cell invasion assay

Cell invasion was analyzed using the Corning BioCoat Matrigel Invasion Chamber kit ((#354480) ThermoFisher Scientific Inc.). Following siRNA transfection, cells were first suspended in Opti-MEM medium. A culture medium with 20% FBS was added (0.6 ml) to the bottom of each transwell of the invasion chamber plate. Suspended cells ($1x10^5$ cells/250 μl) were then added to each transwell insert and allowed to migrate. After forty-eight hours, cells on the upper surface of the transwell were removed using a cotton swab. Migrated cells were fixed with 4% paraformaldehyde in PBS for fifteen minutes and stained with

crystal violet solution for ten minutes (Justus et al., 2014, Zhang et al., 2020). After washing with distilled water, the inserts were digitally imaged using a Zeiss stereo-microscope with an attached AxioCam MRC-5 digital camera (Zeiss, Jena Germany). Migrated cells were counted within four separate areas of the insert; an average number of migrated cells was calculated (Pijuan et al., 2019). Each experiment was repeated three times with triplicates for each treatment group.

Flow cytometry and cell cycle analysis

Seeded at a density of $2x10^5$ cells per well in triplicate in six-well plates, iHEECs were transfected with *NT* or *EGR1* targeted siRNAs. Forty-eight hours post-transfection, cells were harvested, washed with PBS, fixed in 70% chilled ethanol, before staining with propidium iodide (PI)/RNase staining solution (#4087, Cell Signaling Technology Inc.). Analysis of cell cycle stage was conducted using a flow cytometer (Attune NXT Acoustic Focusing Flow Cytometer, Invitrogen) with installed FlowJo software (version 10.7.1). Cell cycle analysis experiments were performed in triplicate and repeated three times.

Statistical analysis

Two-tailed unpaired Student *t*-tests were used to estimate the statistical significance of differences between the two groups. Unless otherwise stated, data were graphically presented as mean ± standard error of the mean (SEM). Differences with *p*-values <0.05 were considered statistically significant; asterisks represent the level of significance: *$p<0.05$, **$p<0.01$, ***$p<0.001$, and ****$p<0.0001$. Prism software version 9 (GraphPad Software Inc., San Diego CA) was used for the majority of the reported statistical analyses.

Results

Expression of EGR1 is significantly increased in Baboon endometriotic lesions

Analyses of published microarray datasets from human endometriotic tissues compared with matched eutopic endometria revealed that *EGR1* transcript levels are significantly elevated in ovarian endometrioma when compared to matched eutopic endometrium (Hever et al., 2007, Crispi et al., 2013) (Supplementary Fig. 1), suggesting a possible link between aberrant *EGR1* expression and endometriosis pathology progression. This supposition is supported by the observed increase in EGR1 protein expression in the glandular epithelial and stromal compartments within endometriotic lesions in a baboon model for experimental induced endometriosis (Fazleabas, 2006b, Fazleabas, 2006a) (Fig. 1). Noteworthy, the surrounding host tissue also scores positive for EGR1 immunopositivity; however, the staining is less intense as compared with the endometriotic lesion. Because the host microenvironment (*i.e.* the reactive stromal environment) is expected to display an inflammatory response (Wilson, 2018), and because EGR1 is induced by inflammatory stimuli (Bhattacharyya et al., 2011), it's not unexpected that EGR1 expression levels would increase within the surrounding host microenvironment in response to local ectopic lesion development.

Pathogenic properties of human epithelial endometriotic cells require EGR1

Based on our histological findings (Fig. 1), we investigated whether EGR1 is required for the proliferative, migratory, and invasive properties of a cultured human epithelial endometriotic cell line (iHEEC (Bono et al., 2012)). A 50-60% reduction in *EGR1* transcript levels was shown to result in a marked attenuation in iHEEC proliferation (Fig. 2A), a significantly reduced number of colonies were also observed with iHEECs following *EGR1* knockdown (Fig. 2B). Linked to the aforementioned, cell cycle analyses of iHEECs with reduced EGR1 levels demonstrate that a significant number of these cells are arrested during the S-phase of the cell cycle (Supplementary Fig. 2). Note that these changes in cellular properties of the iHEEC line are solely due to changes in EGR1 levels and not due to alteration in levels of other members of the EGR family (Supplementary Fig. 3). Endogenous EGR1 expression levels also are required to maintain the full migratory and invasive properties of the iHEEC line (Figs. 3 and 4). Because EGR1 is highly expressed in stromal cells of ectopic endometriotic lesions, we also demonstrated that maintenance of EGR1 expression levels in a recently generated hTERT-immortalized human stromal endometriotic cell line (iEc-ESC) (Song et al., 2020a) is required for its full pathogenic cellular properties (Supplementary Fig. 4). Collectively, the above findings provide strong support for critical roles for both epithelial- and stromal-derived EGR1 in the pathogenic properties of endometriotic lesions.

Transcriptomic changes in iHEECs in response to decreased EGR1 levels

Because EGR1 is a transcription factor, genome-wide RNA profiling was conducted to identify the downstream genes, pathways and networks that may mediate EGR1's role in the above pathogenic properties of iHEECs. The experimental design for the RNA-seq study is schematically shown (Fig. 5A). Briefly, cultured iHEECs in six-well plates were transfected with *NT* or *EGR1* targeted siRNAs forty-eight hours before RNA isolation and sequencing; triplicate samples were used per treatment group. All genes differentially expressed between *NT* and *EGR1* siRNA treated iHEEC groups are tabulated in an Excel spreadsheet in the supplementary section (Supplementary Folder 1), also included in this folder is the gene ontology (GO) analysis by DAVID for sets of differentially expressed genes. As expected, the expression of the EGR1 gene is significantly downregulated (Log_2 FC: −2.8) in the differentially expressed gene list (yellow highlighted row).

In total, 22632 (11945 upregulated and 10687 downregulated) expressed genes were detected by RNA-seq (Supplementary Folder 1); 2231 and 1417 genes were significantly upregulated and downregulated respectively. Forty upregulated and thirty-six downregulated genes met the predetermined FDR (≤0.05) and FC (≥1.5) cutoffs. FKPM values for all 22632 genes were analyzed by principal component analysis (PCA (Supplementary Folder 1)). The PCA showed that the *NT* siRNA and *EGR1* siRNA treated groups were significantly separated in terms of their respective triplicates. Tables 2 and 3 list the top 35 genes down and upregulated respecitively that meet the FDR (≤0.05) and FC (≥1.5) cutoffs whereas the expression heatmap (Fig. 5B) shows the top 76 genes (40 upregulated and 36 downregulated) between the *NT* siRNA and *EGR1* siRNA groups with an FDR ≤0.05 and IFCI ≥1.5 cut-off. With *EGR1* knockdown, GSEA showed that pathways involved in inflammation, estrogen early and late response, adaptation to hypoxia,

epithelial-mesenchymal transition, and cell-cell junctions were significantly enriched (Fig. 6A). Furthermore, DAVID analysis revealed enrichment of biological processes related to cytokine activity, inflammatory response, and cell proliferation and cell death within the differential gene expression set (Fig. 6B). Together, these biological responses are in line with known cellular phenotypes that drive endometriotic lesion progression (Bulun et al., 2019, Taylor et al., 2021).

The volcano plot furnished a global perspective of the transcriptional changes that occur due to EGR1 knockdown (Fig. 7A). To illustrate the diverse functionality of the genes differentially expressed between the *NT* siRNA and *EGR1* siRNA treated groups, 12 genes (10 downregulated genes: Carbonic anhydrase IX (CAIX); diffuse panbronchiolitis critical region 1 (DPCR1); aspartate-rich protein 1 (DRICH1); early B-cell factor 2 (EBF2); endogenous retrovirus group 48 member 1 (ERVH48-1); hydroxycarboxylic acid receptor 3 (HCAR3); interleukin-6 (IL6); metallothionein 1G (MT1G); serpin A9 (SEPINA9); serpin B4 (SERPINB4); and 2 upregulated: phospholipid phosphatase related 1 (PLPPR1) and synapsin 2 (SYN2)) are highlighted in the volcano plot that are significantly differentially expressed in iHEECs following *EGR1* knockdown (Fig. 7A). In addition, the differential expression of these genes in iHEECs following *EGR1* knockdown was validated at the RNA level by qRT-PCR (Fig. 7B).

The pathogenic cellular properties of iHEECs require CAIX

The CAIX gene was further validated to showcase the usefulness of this EGR1 transcriptome dataset in identifying potential new pathogenic molecular mediators of endometriosis (Fig. 8). Analysis of published human endometriotic microarray datasets (Gene Expression Omnibus dataset GSE25628 (Crispi et al., 2013)) reveals that *CAIX* transcript levels are significantly increased in ectopic endometriotic lesions when compared to eutopic endometrial tissue (Fig. 8A). Immunohistochemical studies also show that CAIX protein is significantly expressed in epithelial cells of baboon ectopic endometriotic lesions as compared to matched eutopic endometrium (Fig. 8B). Using the iHEEC culture model, we show that CAIX is essential for the pathogenic properties of human endometriotic epithelial cells, which include cellular proliferation, colony formation capability and cell invasion (Fig 8C-H). Together, these results underscore the general utility of the above *EGR1* RNA-seq dataset to uncover new potential drivers of endometriosis progression and highlight CAIX in particular as a molecular EGR1 target that may provide a new perspective in examining the pathogenic properties of endometriotic epithelial cells.

Discussion

As an inflammatory gynecological disorder of reproductive-aged women, endometriosis is diagnosed based on the presence of endometrial-like tissue (epithelial glands and stroma) outside the uterine cavity, usually the abdominal organs and cavities such as the peritoneal mesothelium, ovaries and fallopian tubes (Bulun et al., 2019, Giudice, 2010, Taylor et al., 2021). Superficial peritoneal lesions, deep-infiltrating endometriosis, and ovarian endometriotic cysts (endometriomas) represent the most common anatomic types of pelvic endometriosis. Endometriosis is a debilitating disease, which shares some

characteristics with malignancy, such as cell migration, invasion and adaptation to hypoxia. Severe symptoms of this systemic disorder often include dysmenorrhea, chronic pelvic pain, dyspareunia, infertility, and an elevated risk for ovarian cancer. Although the exact incidence of endometriosis remains uncertain, estimates suggest that the disease affects one in ten women of reproductive age (Simoens et al., 2007), 50-60% of women and teenage girls with pelvic pain (Eskenazi and Warner, 1997), and up to 50% of women with infertility (Ozkan et al., 2008). Despite the adverse impact on a patient's quality of life that can extend well into menopause (Moradi et al., 2014), the etiopathogenesis of endometriosis remains unclear.

For the first time, we provide support for a functional role for the EGR1 transcription factor in the pathogenic properties of human endometriotic cells (epithelial and stromal), which include cell proliferation, migration, and invasion. To our knowledge, EGR1 has not been previously associated with endometriosis. In the case of endometriotic epithelial cells, our RNA-seq analysis identifies a number of biological processes and signaling pathways that may be critical for promoting EGR1-dependent pathogenic cellular processes. Such cellular processes—cell survival, proliferation, migration, and invasion—are essential for endometriotic cells migrating from the menstrual efflux to attach, colonize and invade distant anatomic sites with harsh microenvironments.

Focusing on a subset of molecular targets for which expression levels are downregulated in iHEECs following EGR1 knockdown, we find that many have been implicated in promoting pathologies in other physiological systems. For example, DPCR1—a family member of the major histocompatibility complex class I molecules—has been reported to promote cancer cell proliferation, migration and invasion (Yan et al., 2018). Exclusive to human and higher-order primates, HCAR3 has been correlated with poor long-term survival for patients diagnosed with cancers of the colon (Yang et al., 2021) and cervix (Ding et al., 2020). A member of the serpin superfamily of protease inhibitors, SERPIN A9 has been associated with the cell migration properties of endometriotic cells (Li et al., 2018) whereas SERPIN B4 has been linked to promoting cell proliferation and migration in various cancer cell lines (Heit et al., 2013). As an inflammatory cytokine, IL-6 is involved in a broad spectrum of pathophysiologies (Carmona et al., 2012, Bergqvist et al., 2001, Hirano, 2021), including endometriosis (Song et al., 2020b). A transcription factor containing a non-basic HLH dimerization domain and an atypical zinc-finger DNA–binding domain (Wang et al., 2021b), EBF2 has been linked to a set of pathologies (Li et al., 2019, Mallm et al., 2019, Ng et al., 2020), including endometriosis (Sohler et al., 2013). A member of the metallothionein family (West et al., 1990), MTIG has been associated with the promotion of cell proliferation in many cancer types (Si and Lang, 2018). In aggregate, these findings support EGR1 as a potent transcriptional regulator of diverse signals that individually or together promote the pathogenic properties of endometriotic epithelial cells.

We also provide support for CAIX as a new and important downstream EGR1 target that is critical for maintaining many of the pathogenic properties of endometriotic epithelial cells (Fig. 8). As a membrane-associated zinc metalloenzyme, CAIX was first shown to be upregulated in hypoxic tumors where it plays a central role as an intra- and extra-cellular pH regulator (Pastorekova and Gillies, 2019, Becker, 2020, Benej et al., 2020, Aldera and Govender, 2021, Queen et al., 2022). In hypoxic tumors, CAIX maintains an intracellular

pH (pHi) that is favorable for continued tumor cell growth and survival, while at the same time is involved in generating an acidic extracellular microenvironment that enables tumor cell invasiveness (Shin et al., 2011, Daunys and Petrikaite, 2020). Apart from providing a survival advantage to cancer cells through intracellular neutralization while promoting tumor invasion by extracellular acidification, CAIX has been implicated as essential for modulating cell proliferation, loss of cell adhesion, increased tumor cell migration, invasion, and metastasis (Daunys and Petrikaite, 2020, Shin et al., 2011). Because CAIX is now considered an important molecular marker of poor prognosis in many cancers and diseases (Zamanova et al., 2019), CAIX has attracted increasing attention as a possible drug target to treat various forms of cancers as well as other pathologies (Pastorek and Pastorekova, 2015, Ciccone et al., 2020, Angeli et al., 2020, Supuran, 2020). Considering a growing body of evidence shows that hypoxia regulates the disease phenotype of endometriosis (Kobayashi et al., 2021, Li et al., 2021) and that therapeutic use of CAIX inhibitors has reached phase I clinical trials (McDonald et al., 2020), we believe further investigations on CAIX's involvement in the etiopathogenesis of ectopic endometriotic lesions, and the role of CAIX inhibitors as a treatment option for this disease, is warranted.

In summary, our studies support a critical role for EGR1 in maintaining the pathogenic properties of endometriotic cells through a transcriptome that is derived from a myriad of genes that are known to mediate pathogenic responses in other physiological systems. Future investigations will focus on whether EGR1 inhibitors can be considered a feasible treatment option for endometriosis as shown in other pathological systems (Bhattacharyya et al., 2011). The fact that the use of an EGR1 inhibitor (mithramycin) has reached a phase I/II clinical trial for certain cancer types (Grohar et al., 2017), and that we have shown that mithramycin significantly suppresses the pathogenic cellular properties of the iHEEC line (data not shown), provide additional motivation to further study EGR1 inhibitors in the context of endometriosis treatment in the future. An important focus will also be the identification of the transcriptome that mediates EGR1's pathogenic responses in endometriotic stromal cells and identify the commonalities and differences between the EGR1 transcriptomes derived from human endometriotic epithelial and stromal cells. Finally, these *in vitro* findings will need to be functionally validated *in vivo* using established animal models for experimental endometriosis in the future.

Supplementary Material

Refer to Web version on PubMed Central for supplementary material.

Acknowledgements

We thank Yan Ying and Rong Zhao for their technical assistance. The iHEEC line was kindly provided by Dr. Sang Jun Han, Baylor College of Medicine, Houston, Texas USA. This project was supported in part by the Cytometry and Cell Sorting Core at Baylor College of Medicine with funding from the NIH (AI036211; CA125123; and RR024574). This project was also supported in part by the Genomic and RNA Profiling Core at Baylor College of Medicine with funding from the NIH NCI (P30CA125123) and CPRIT (RP200504) grants. Finally, we thank CD Genomics, Shirley, New York USA for contributing to part of the bioinformatic analysis reported in this study.

Funding

This research was funded by the National Institutes of Health (NIH)/ National Institute of Child Health Development (NICHD) grants: R01 HD-099090 to ATF and R01 HD-042311 to JPL.

References

Aldera AP & Govender D 2021 Carbonic anhydrase IX: a regulator of pH and participant in carcinogenesis. J Clin Pathol.(10.1136/jclinpath-2020-207073)

Anders S, Pyl PT & Huber W 2015 HTSeq--a Python framework to work with high-throughput sequencing data. Bioinformatics 31 166–9.(10.1093/bioinformatics/btu638) [PubMed: 25260700]

Angeli A, Carta F, Nocentini A, Winum JY, Zalubovskis R, Akdemir A, Onnis V, Eldehna WM, Capasso C, Simone G, et al. 2020 Carbonic Anhydrase Inhibitors Targeting Metabolism and Tumor Microenvironment. Metabolites 10.(10.3390/metabo10100412)

Becker HM 2020 Carbonic anhydrase IX and acid transport in cancer. Br J Cancer 122 157–167. (10.1038/s41416-019-0642-z) [PubMed: 31819195]

Benej M, Svastova E, Banova R, Kopacek J, Gibadulinova A, Kery M, Arena S, Scaloni A, Vitale M, Zambrano N, et al. 2020 CA IX Stabilizes Intracellular pH to Maintain Metabolic Reprogramming and Proliferation in Hypoxia. Front Oncol 10 1462.(10.3389/fonc.2020.01462) [PubMed: 32983978]

Benjamini Y, Hochberg Y 1995 Controlling the false discovery rate: a practical and powerful approach to multiple testing. Statistical Society B57 289–300.

Benos PV, Lapedes AS & Stormo GD 2002 Probabilistic code for DNA recognition by proteins of the EGR family. J Mol Biol 323 701–27.(10.1016/s0022-2836(02)00917-8) [PubMed: 12419259]

Bergqvist A, Bruse C, Carlberg M & Carlstrom K 2001 Interleukin 1beta, interleukin-6, and tumor necrosis factor-alpha in endometriotic tissue and in endometrium. Fertil Steril 75 489–95.(10.1016/s0015-0282(00)01752-0) [PubMed: 11239529]

Bhattacharyya S, Wu M, Fang F, Tourtellotte W, Feghali-Bostwick C & Varga J 2011 Early growth response transcription factors: key mediators of fibrosis and novel targets for anti-fibrotic therapy. Matrix Biol 30 235–42.(10.1016/j.matbio.2011.03.005) [PubMed: 21511034]

Bono Y, Kyo S, Takakura M, Maida Y, Mizumoto Y, Nakamura M, Nomura K, Kiyono T & Inoue M 2012 Creation of immortalised epithelial cells from ovarian endometrioma. Br J Cancer 106 1205–13.(10.1038/bjc.2012.26) [PubMed: 22353808]

Bulun SE, Yilmaz BD, Sison C, Miyazaki K, Bernardi L, Liu S, Kohlmeier A, Yin P, Milad M & Wei J 2019 Endometriosis. Endocr Rev 40 1048–1079.(10.1210/er.2018-00242) [PubMed: 30994890]

Cagle P, Niture S, Srivastava A, Ramalinga M, Aqeel R, Rios-Colon L, Chimeh U, Suy S, Collins SP, Dahiya R, et al. 2019 MicroRNA-214 targets PTK6 to inhibit tumorigenic potential and increase drug sensitivity of prostate cancer cells. Sci Rep 9 9776.(10.1038/s41598-019-46170-3) [PubMed: 31278310]

Campling BG, Pym J, Galbraith PR & Cole SP 1988 Use of the MTT assay for rapid determination of chemosensitivity of human leukemic blast cells. Leuk Res 12 823–31. (10.1016/0145-2126(88)90036-7) [PubMed: 3199842]

Carmona F, Chapron C, Martinez-Zamora MA, Santulli P, Rabanal A, Martinez-Florensa M, Lozano F & Balasch J 2012 Ovarian endometrioma but not deep infiltrating endometriosis is associated with increased serum levels of interleukin-8 and interleukin-6. J Reprod Immunol 95 80–6.(10.1016/j.jri.2012.06.001) [PubMed: 22819248]

Ciccone V, Filippelli A, Angeli A, Supuran CT & Morbidelli L 2020 Pharmacological Inhibition of CA-IX Impairs Tumor Cell Proliferation, Migration and Invasiveness. Int J Mol Sci 21.(10.3390/ijms21082983)

Crispi S, Piccolo MT, D'avino A, Donizetti A, Viceconte R, Spyrou M, Calogero RA, Baldi A & Signorile PG 2013 Transcriptional profiling of endometriosis tissues identifies genes related to organogenesis defects. J Cell Physiol 228 1927–34.(10.1002/jcp.24358) [PubMed: 23460397]

D'hooghe TM, Bambra CS, Suleman MA, Dunselman GA, Evers HL & Koninckx PR 1994 Development of a model of retrograde menstruation in baboons (Papio anubis). Fertil Steril 62 635–8. [PubMed: 8062962]

Daunys S & Petrikaite V 2020 The roles of carbonic anhydrases IX and XII in cancer cell adhesion, migration, invasion and metastasis. Biol Cell 112 383–397.(10.1111/boc.201900099) [PubMed: 32894882]

Ding H, Xiong XX, Fan GL, Yi YX, Chen YR, Wang JT & Zhang W 2020 The New Biomarker for Cervical Squamous Cell Carcinoma and Endocervical Adenocarcinoma (CESC) Based on Public Database Mining. Biomed Res Int 2020 5478574.(10.1155/2020/5478574) [PubMed: 32351997]

Dobin A, Davis CA, Schlesinger F, Drenkow J, Zaleski C, Jha S, Batut P, Chaisson M & Gingeras TR 2013 STAR: ultrafast universal RNA-seq aligner. Bioinformatics 29 15–21.(10.1093/bioinformatics/bts635) [PubMed: 23104886]

Eskenazi B & Warner ML 1997 Epidemiology of endometriosis. Obstet Gynecol Clin North Am 24 235–58.(10.1016/s0889-8545(05)70302-8) [PubMed: 9163765]

Fazleabas AT 2006a A baboon model for inducing endometriosis. Methods Mol Med 121 95–9.(10.1385/1-59259-983-4:093) [PubMed: 16251737]

Fazleabas AT 2006b A baboon model for simulating pregnancy. Methods Mol Med 121 101–10.(10.1385/1-59259-983-4:099) [PubMed: 16251738]

Fazleabas AT, Brudney A, Gurates B, Chai D & Bulun S 2002 A modified baboon model for endometriosis. Ann N Y Acad Sci 955 308–17; discussion 340-2, 396-406.(10.1111/j.1749-6632.2002.tb02791.x) [PubMed: 11949957]

Gashler A & Sukhatme VP 1995 Early growth response protein 1 (Egr-1): prototype of a zinc-finger family of transcription factors. Prog Nucleic Acid Res Mol Biol 50 191–224.(10.1016/s0079-6603(08)60815-6) [PubMed: 7754034]

Giudice LC 2010 Clinical practice. Endometriosis. N Engl J Med 362 2389–98.(10.1056/NEJMcp1000274) [PubMed: 20573927]

Grada A, Otero-Vinas M, Prieto-Castrillo F, Obagi Z & Falanga V 2017 Research Techniques Made Simple: Analysis of Collective Cell Migration Using the Wound Healing Assay. J Invest Dermatol 137 e11–e16.(10.1016/j.jid.2016.11.020) [PubMed: 28110712]

Grohar PJ, Glod J, Peer CJ, Sissung TM, Arnaldez FI, Long L, Figg WD, Whitcomb P, Helman LJ & Widemann BC 2017 A phase I/II trial and pharmacokinetic study of mithramycin in children and adults with refractory Ewing sarcoma and EWS-FLI1 fusion transcript. Cancer Chemother Pharmacol 80 645–652.(10.1007/s00280-017-3382-x) [PubMed: 28735378]

Guo B, Tian XC, Li DD, Yang ZQ, Cao H, Zhang QL, Liu JX & Yue ZP 2014 Expression, regulation and function of Egr1 during implantation and decidualization in mice. Cell Cycle 13 2626–40.(10.4161/15384101.2014.943581) [PubMed: 25486203]

Gururajan M, Simmons A, Dasu T, Spear BT, Calulot C, Robertson DA, Wiest DL, Monroe JG & Bondada S 2008 Early growth response genes regulate B cell development, proliferation, and immune response. J Immunol 181 4590–602.(10.4049/jimmunol.181.7.4590) [PubMed: 18802061]

Han SJ, Hawkins SM, Begum K, Jung SY, Kovanci E, Qin J, Lydon JP, Demayo FJ & O'malley BW 2012 A new isoform of steroid receptor coactivator-1 is crucial for pathogenic progression of endometriosis. Nat Med 18 1102–11.(10.1038/nm.2826) [PubMed: 22660634]

Hao L, Huang F, Yu X, Xu B, Liu Y, Zhang Y & Zhu Y 2021 The Role of Early Growth Response Family Members 1-4 in Prognostic Value of Breast Cancer. Front Genet 12 680132.(10.3389/fgene.2021.680132) [PubMed: 34178038]

Heit C, Jackson BC, Mcandrews M, Wright MW, Thompson DC, Silverman GA, Nebert DW & Vasiliou V 2013 Update of the human and mouse SERPIN gene superfamily. Hum Genomics 7 22.(10.1186/1479-7364-7-22) [PubMed: 24172014]

Hever A, Roth RB, Hevezi P, Marin ME, Acosta JA, Acosta H, Rojas J, Herrera R, Grigoriadis D, White E, et al. 2007 Human endometriosis is associated with plasma cells and overexpression of B lymphocyte stimulator. Proc Natl Acad Sci U S A 104 12451–6.(10.1073/pnas.0703451104) [PubMed: 17640886]

Hirano T 2021 IL-6 in inflammation, autoimmunity and cancer. Int Immunol 33 127–148.(10.1093/intimm/dxaa078) [PubMed: 33337480]

Huang Da W, Sherman BT & Lempicki RA 2009 Systematic and integrative analysis of large gene lists using DAVID bioinformatics resources. Nat Protoc 4 44–57.(10.1038/nprot.2008.211) [PubMed: 19131956]

Justus CR, Leffler N, Ruiz-Echevarria M & Yang LV 2014 In vitro cell migration and invasion assays. J Vis Exp.(10.3791/51046)

Kim HR, Kim YS, Yoon JA, Lyu SW, Shin H, Lim HJ, Hong SH, Lee DR & Song H 2014 Egr1 is rapidly and transiently induced by estrogen and bisphenol A via activation of nuclear estrogen receptor-dependent ERK1/2 pathway in the uterus. Reprod Toxicol 50 60–7.(10.1016/j.reprotox.2014.10.010) [PubMed: 25461906]

Kim HR, Kim YS, Yoon JA, Yang SC, Park M, Seol DW, Lyu SW, Jun JH, Lim HJ, Lee DR, et al. 2018 Estrogen induces EGR1 to fine-tune its actions on uterine epithelium by controlling PR signaling for successful embryo implantation. FASEB J 32 1184–1195.(10.1096/fj.201700854RR) [PubMed: 29092905]

Kobayashi H, Shigetomi H & Imanaka S 2021 Nonhormonal therapy for endometriosis based on energy metabolism regulation. Reprod Fertil 2 C42–C57.(10.1530/RAF-21-0053) [PubMed: 35118411]

Kommagani R, Szwarc MM, Kovanci E, Gibbons WE, Putluri N, Maity S, Creighton CJ, Sreekumar A, Demayo FJ, Lydon JP, et al. 2013 Acceleration of the glycolytic flux by steroid receptor coactivator-2 is essential for endometrial decidualization. PLoS Genet 9 e1003900.(10.1371/journal.pgen.1003900) [PubMed: 24204309]

Kommagani R, Szwarc MM, Vasquez YM, Peavey MC, Mazur EC, Gibbons WE, Lanz RB, Demayo FJ & Lydon JP 2016 The Promyelocytic Leukemia Zinc Finger Transcription Factor Is Critical for Human Endometrial Stromal Cell Decidualization. PLoS Genet 12 e1005937.(10.1371/journal.pgen.1005937) [PubMed: 27035670]

Lee SL, Sadovsky Y, Swirnoff AH, Polish JA, Goda P, Gavrilina G & Milbrandt J 1996 Luteinizing hormone deficiency and female infertility in mice lacking the transcription factor NGFI-A (Egr-1). Science 273 1219–21.(10.1126/science.273.5279.1219) [PubMed: 8703054]

Li M, Shen Y, Wang Q & Zhou X 2019 MiR-204-5p promotes apoptosis and inhibits migration of osteosarcoma via targeting EBF2. Biochimie 158 224–232.(10.1016/j.biochi.2018.12.003) [PubMed: 30529043]

Li W, Fan X, Zhang M, Huang L, Lv S, Wang L, Wu Y, Dai C, Xu J, Xu P, et al. 2018 Systematic analysis of hsa-miR-363 gene overexpression pattern in endometrial stromal cells. Int J Mol Med 42 2793–2800.(10.3892/ijmm.2018.3840) [PubMed: 30226573]

Li WN, Wu MH & Tsai SJ 2021 HYPOXIA AND REPRODUCTIVE HEALTH: The role of hypoxia in the development and progression of endometriosis. Reproduction 161 F19–F31.(10.1530/REP-20-0267) [PubMed: 33112784]

Liang XH, Deng WB, Li M, Zhao ZA, Wang TS, Feng XH, Cao YJ, Duan EK & Yang ZM 2014 Egr1 protein acts downstream of estrogen-leukemia inhibitory factor (LIF)-STAT3 pathway and plays a role during implantation through targeting Wnt4. J Biol Chem 289 23534–45.(10.1074/jbc.M114.588897) [PubMed: 25012664]

Liberzon A, Subramanian A, Pinchback R, Thorvaldsdottir H, Tamayo P & Mesirov JP 2011 Molecular signatures database (MSigDB) 3.0. Bioinformatics 27 1739–40.(10.1093/bioinformatics/btr260) [PubMed: 21546393]

Ma Z, Gao X, Shuai Y, Wu X, Yan Y, Xing X & Ji J 2021 EGR1-mediated linc01503 promotes cell cycle progression and tumorigenesis in gastric cancer. Cell Prolif 54 e12922.(10.1111/cpr.12922) [PubMed: 33145887]

Madden SL & Rauscher FJ 3rd 1993 Positive and negative regulation of transcription and cell growth mediated by the EGR family of zinc-finger gene products. Ann N Y Acad Sci 684 75–84.(10.1111/j.1749-6632.1993.tb32272.x) [PubMed: 8317848]

Mallm JP, Iskar M, Ishaque N, Klett LC, Kugler SJ, Muino JM, Teif VB, Poos AM, Grossmann S, Erdel F, et al. 2019 Linking aberrant chromatin features in chronic lymphocytic leukemia to transcription factor networks. Mol Syst Biol 15 e8339.(10.15252/msb.20188339) [PubMed: 31118277]

Mcdonald PC, Chia S, Bedard PL, Chu Q, Lyle M, Tang L, Singh M, Zhang Z, Supuran CT, Renouf DJ, et al. 2020 A Phase 1 Study of SLC-0111, a Novel Inhibitor of Carbonic Anhydrase IX, in Patients With Advanced Solid Tumors. Am J Clin Oncol 43 484–490.(10.1097/COC.0000000000000691) [PubMed: 32251122]

Mootha VK, Lindgren CM, Eriksson KF, Subramanian A, Sihag S, Lehar J, Puigserver P, Carlsson E, Ridderstrale M, Laurila E, et al. 2003 PGC-1alpha-responsive genes involved in oxidative phosphorylation are coordinately downregulated in human diabetes. Nat Genet 34 267–73.(10.1038/ng1180) [PubMed: 12808457]

Moradi M, Parker M, Sneddon A, Lopez V & Ellwood D 2014 Impact of endometriosis on women's lives: a qualitative study. BMC Womens Health 14 123.(10.1186/1472-6874-14-123) [PubMed: 25280500]

Mosmann T 1983 Rapid colorimetric assay for cellular growth and survival: application to proliferation and cytotoxicity assays. J Immunol Methods 65 55–63.(10.1016/0022-1759(83)90303-4) [PubMed: 6606682]

Ng AP, Coughlan HD, Hediyeh-Zadeh S, Behrens K, Johanson TM, Low MSY, Bell CC, Gilan O, Chan YC, Kueh AJ, et al. 2020 An Erg-driven transcriptional program controls B cell lymphopoiesis. Nat Commun 11 3013.(10.1038/s41467-020-16828-y) [PubMed: 32541654]

O'donovan KJ, Tourtellotte WG, Millbrandt J & Baraban JM 1999 The EGR family of transcription-regulatory factors: progress at the interface of molecular and systems neuroscience. Trends Neurosci 22 167–73.(10.1016/s0166-2236(98)01343-5) [PubMed: 10203854]

Ozkan S, Murk W & Arici A 2008 Endometriosis and infertility: epidemiology and evidence-based treatments. Ann N Y Acad Sci 1127 92–100.(10.1196/annals.1434.007) [PubMed: 18443335]

Pastorek J & Pastorekova S 2015 Hypoxia-induced carbonic anhydrase IX as a target for cancer therapy: from biology to clinical use. Semin Cancer Biol 31 52–64.(10.1016/j.semcancer.2014.08.002) [PubMed: 25117006]

Pastorekova S & Gillies RJ 2019 The role of carbonic anhydrase IX in cancer development: links to hypoxia, acidosis, and beyond. Cancer Metastasis Rev 38 65–77.(10.1007/s10555-019-09799-0) [PubMed: 31076951]

Pijuan J, Barcelo C, Moreno DF, Maiques O, Siso P, Marti RM, Macia A & Panosa A 2019 In vitro Cell Migration, Invasion, and Adhesion Assays: From Cell Imaging to Data Analysis. Front Cell Dev Biol 7 107.(10.3389/fcell.2019.00107) [PubMed: 31259172]

Queen A, Bhutto HN, Yousuf M, Syed MA & Hassan MI 2022 Carbonic anhydrase IX: A tumor acidification switch in heterogeneity and chemokine regulation. Semin Cancer Biol.(10.1016/j.semcancer.2022.01.001)

Robinson MD, Mccarthy DJ & Smyth GK 2010 edgeR: a Bioconductor package for differential expression analysis of digital gene expression data. Bioinformatics 26 139–40.(10.1093/bioinformatics/btp616) [PubMed: 19910308]

Sherman BT, Huang Da W, Tan Q, Guo Y, Bour S, Liu D, Stephens R, Baseler MW, Lane HC & Lempicki RA 2007 DAVID Knowledgebase: a gene-centered database integrating heterogeneous gene annotation resources to facilitate high-throughput gene functional analysis. BMC Bioinformatics 8 426.(10.1186/1471-2105-8-426) [PubMed: 17980028]

Shin HJ, Rho SB, Jung DC, Han IO, Oh ES & Kim JY 2011 Carbonic anhydrase IX (CA9) modulates tumor-associated cell migration and invasion. J Cell Sci 124 1077–87.(10.1242/jcs.072207) [PubMed: 21363891]

Si M & Lang J 2018 The roles of metallothioneins in carcinogenesis. J Hematol Oncol 11 107.(10.1186/s13045-018-0645-x) [PubMed: 30139373]

Simoens S, Hummelshoj L & D'hooghe T 2007 Endometriosis: cost estimates and methodological perspective. Hum Reprod Update 13 395–404.(10.1093/humupd/dmm010) [PubMed: 17584822]

Sohler F, Sommer A, Wachter DL, Agaimy A, Fischer OM, Renner SP, Burghaus S, Fasching PA, Beckmann MW, Fuhrmann U, et al. 2013 Tissue remodeling and nonendometrium-like menstrual cycling are hallmarks of peritoneal endometriosis lesions. Reprod Sci 20 85–102.(10.1177/1933719112451147) [PubMed: 22878529]

Song Y, Joshi NR, Vegter E, Hrbek S, Lessey BA & Fazleabas AT 2020a Establishment of an Immortalized Endometriotic Stromal Cell Line from Human Ovarian Endometrioma. Reprod Sci 27 2082–2091.(10.1007/s43032-020-00228-0) [PubMed: 32542539]

Song Y, Su RW, Joshi NR, Kim TH, Lessey BA, Jeong JW & Fazleabas AT 2020b Interleukin-6 (IL-6) Activates the NOTCH1 Signaling Pathway Through E-Proteins in Endometriotic Lesions. J Clin Endocrinol Metab 105.(10.1210/clinem/dgaa096)

Subramanian A, Tamayo P, Mootha VK, Mukherjee S, Ebert BL, Gillette MA, Paulovich A, Pomeroy SL, Golub TR, Lander ES, et al. 2005 Gene set enrichment analysis: a knowledge-based approach for interpreting genome-wide expression profiles. Proc Natl Acad Sci U S A 102 15545–50. (10.1073/pnas.0506580102) [PubMed: 16199517]

Sukhatme VP 1990 Early transcriptional events in cell growth: the Egr family. J Am Soc Nephrol 1 859–66.(10.1681/ASN.V16859) [PubMed: 2129480]

Supuran CT 2020 Experimental Carbonic Anhydrase Inhibitors for the Treatment of Hypoxic Tumors. J Exp Pharmacol 12 603–617.(10.2147/JEP.S265620) [PubMed: 33364855]

Swirnoff AH & Milbrandt J 1995 DNA-binding specificity of NGFI-A and related zinc finger transcription factors. Mol Cell Biol 15 2275–87.(10.1128/MCB.15.4.2275) [PubMed: 7891721]

Szwarc MM, Hai L, Gibbons WE, Mo Q, Lanz RB, Demayo FJ & Lydon JP 2019 Early growth response 1 transcriptionally primes the human endometrial stromal cell for decidualization. J Steroid Biochem Mol Biol 189 283–290.(10.1016/j.jsbmb.2019.01.021) [PubMed: 30711473]

Szwarc MM, Hai L, Gibbons WE, Peavey MC, White LD, Mo Q, Lonard DM, Kommagani R, Lanz RB, Demayo FJ, et al. 2018a Human endometrial stromal cell decidualization requires transcriptional reprogramming by PLZF. Biol Reprod 98 15–27.(10.1093/biolre/iox161) [PubMed: 29186366]

Szwarc MM, Hai L, Gibbons WE, White LD, Mo Q, Kommagani R, Lanz RB, Demayo FJ, O'malley BW & Lydon JP 2018b Retinoid signaling controlled by SRC-2 in decidualization revealed by transcriptomics. Reproduction 156 387–395.(10.1530/REP-18-0282) [PubMed: 30325183]

Taylor HS, Kotlyar AM & Flores VA 2021 Endometriosis is a chronic systemic disease: clinical challenges and novel innovations. Lancet 397 839–852.(10.1016/S0140-6736(21)00389-5) [PubMed: 33640070]

Todaro GJ, Lazar GK & Green H 1965 The initiation of cell division in a contact-inhibited mammalian cell line. J Cell Physiol 66 325–33.(10.1002/jcp.1030660310) [PubMed: 5884360]

Topilko P, Schneider-Maunoury S, Levi G, Trembleau A, Gourdji D, Driancourt MA, Rao CV & Charnay P 1998 Multiple pituitary and ovarian defects in Krox-24 (NGFI-A, Egr-1)-targeted mice. Mol Endocrinol 12 107–22.(10.1210/mend.12.1.0049) [PubMed: 9440815]

Wang B, Guo H, Yu H, Chen Y, Xu H & Zhao G 2021a The Role of the Transcription Factor EGR1 in Cancer. Front Oncol 11 642547.(10.3389/fonc.2021.642547) [PubMed: 33842351]

Wang Q, Liang J, Hu X, Gu S, Xu Q & Yan J 2021b Early B-cell factors involve in the tumorigenesis and predict the overall survival of gastric cancer. Biosci Rep 41.(10.1042/BSR20210055)

West AK, Stallings R, Hildebrand CE, Chiu R, Karin M & Richards RI 1990 Human metallothionein genes: structure of the functional locus at 16q13. Genomics 8 513–8. (10.1016/0888-7543(90)90038-v) [PubMed: 2286373]

Wilson RB 2018 Hypoxia, cytokines and stromal recruitment: parallels between pathophysiology of encapsulating peritoneal sclerosis, endometriosis and peritoneal metastasis. Pleura Peritoneum 3 20180103.(10.1515/pp-2018-0103) [PubMed: 30911653]

Wolfe MW & Call GB 1999 Early growth response protein 1 binds to the luteinizing hormone-beta promoter and mediates gonadotropin-releasing hormone-stimulated gene expression. Mol Endocrinol 13 752–63.(10.1210/mend.13.5.0276) [PubMed: 10319325]

Yan J, Chen G, Zhao X, Chen F, Wang T & Miao F 2018 High expression of diffuse panbronchiolitis critical region 1 gene promotes cell proliferation, migration and invasion in pancreatic ductal adenocarcinoma. Biochem Biophys Res Commun 495 1908–1914.(10.1016/j.bbrc.2017.12.031) [PubMed: 29242154]

Yan J, Gao Y, Lin S, Li Y, Shi L & Kan Q 2021 EGR1-CCL2 Feedback Loop Maintains Epithelial-Mesenchymal Transition of Cisplatin-Resistant Gastric Cancer Cells and Promotes Tumor Angiogenesis. Dig Dis Sci.(10.1007/s10620-021-07250-5)

Yan SF, Fujita T, Lu J, Okada K, Shan Zou Y, Mackman N, Pinsky DJ & Stern DM 2000 Egr-1, a master switch coordinating upregulation of divergent gene families underlying ischemic stress. Nat Med 6 1355–61.(10.1038/82168) [PubMed: 11100120]

Yang X, Wei W, Tan S, Guo L, Qiao S, Yao B & Wang Z 2021 Identification and verification of HCAR3 and INSL5 as new potential therapeutic targets of colorectal cancer. World J Surg Oncol 19 248.(10.1186/s12957-021-02335-x) [PubMed: 34419055]

Zamanova S, Shabana AM, Mondal UK & Ilies MA 2019 Carbonic anhydrases as disease markers. Expert Opin Ther Pat 29 509–533.(10.1080/13543776.2019.1629419) [PubMed: 31172829]

Zhang F, Liu R, Zhang H, Liu C, Liu C & Lu Y 2020 Suppressing Dazl modulates tumorigenicity and stemness in human glioblastoma cells. BMC Cancer 20 673.(10.1186/s12885-020-07155-y) [PubMed: 32682409]

Zhang L, Ren R, Yang X, Ge Y, Zhang X & Yuan H 2021 Oncogenic role of early growth response-1 in liver cancer through the regulation of the microRNA-675/sestrin 3 and the Wnt/beta-catenin signaling pathway. Bioengineered 12 5305–5322.(10.1080/21655979.2021.1964889) [PubMed: 34409922]

Zhang Y, Ji G, Han S, Shao Z, Lu Z, Huo L, Zhang J, Yang R, Feng Q, Shen H, et al. 2018 Tip60 Suppresses Cholangiocarcinoma Proliferation and Metastasis via PI3k-AKT. Cell Physiol Biochem 50 612–628.(10.1159/000494183) [PubMed: 30308494]

Zhao J, Li H & Yuan M 2021 EGR1 promotes stemness and predicts a poor outcome of uterine cervical cancer by inducing SOX9 expression. Genes Genomics 43 459–470.(10.1007/s13258-021-01064-5) [PubMed: 33687657]

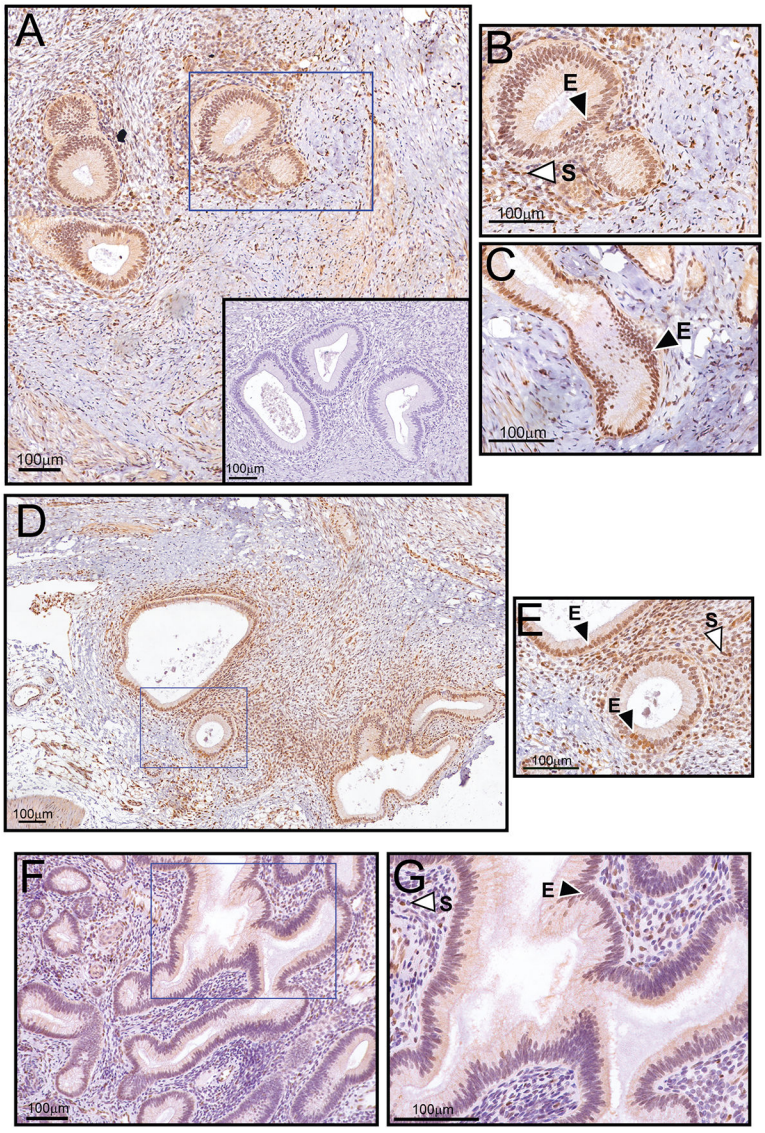

Figure 1.

Significant EGR1 protein expression in epithelial and stromal cells of baboon ectopic endometriotic lesions. (A) Low power magnification image of an endometriotic lesion biopsied from the pelvic region of the baboon. Note the strong expression of EGR1 in the glandular epithelium and underlying stroma. The inset shows negative control staining, which does not include the primary antibody against EGR1. (B) Higher magnification image of a region demarcated with a blue box in (A); the epithelium and stroma are denoted by “E” and “S” respectively. (C) Higher magnification image of an elongated epithelial gland within the same endometriotic lesion (outside the field shown in (A)). Again, note the marked immunoreactivity for EGR1 in all epithelial cells that comprise the gland. (D) Low power magnification image of an endometriotic lesion in the peritoneal region. Again, note the significant EGR1 immunopositivity within the endometriotic lesion. (E) Higher power magnification image of a region delineated by the blue box in (D). Again, note the strong expression for EGR1 in the epithelial and stromal compartments that comprise the

endometriotic lesion. (F) Matched eutopic endometrium exhibits significantly lower EGR1 expression in the epithelial and stromal compartments. (G) Higher magnification image of the region outlined by the blue box in (F). Note that the eutopic uterus and both ectopic endometriotic lesions shown are derived from the same animal during the secretory phase of the cycle (see: Materials and methods sub-section). The data are representative of a group size of n=4.

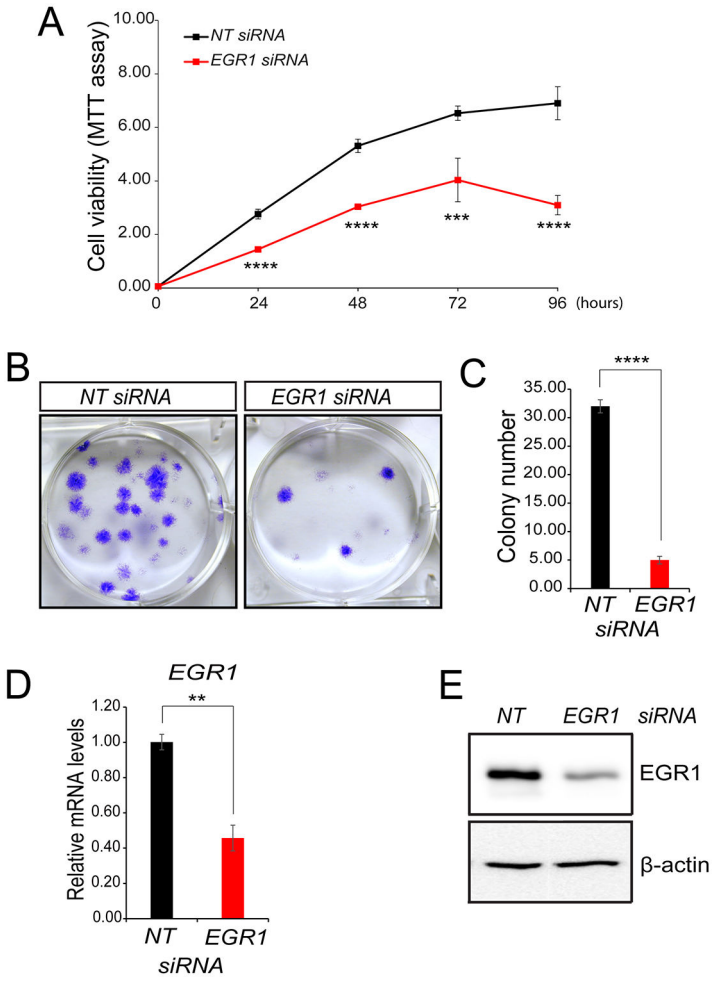

Figure 2.

Proliferative and colony-forming properties of human endometriotic epithelial cells require EGR1. (A) Following *NT* or *EGR1* siRNA transfection, iHEEC viability was assessed by the MTT assay. (B) A representative result from a colony-formation assay to assess the colony-forming abilities of human endometriotic epithelial cells forty-eight hours following *NT* or *EGR1* siRNA transfection and subsequent culture for 10 days. (C) The histogram displays quantification of stained colony numbers. (D-E) Representative results of qPCR and Western immunoblot analyses confirm EGR1 depletion in the iHEEC line. For Western analyses, β-actin was used as a control for protein loading. Results are indicated as mean ± SE and are representative of three independent experiments; ** *p*-value<0.01; *** *p*-value<0.001; and **** *p*-value<0.0001.

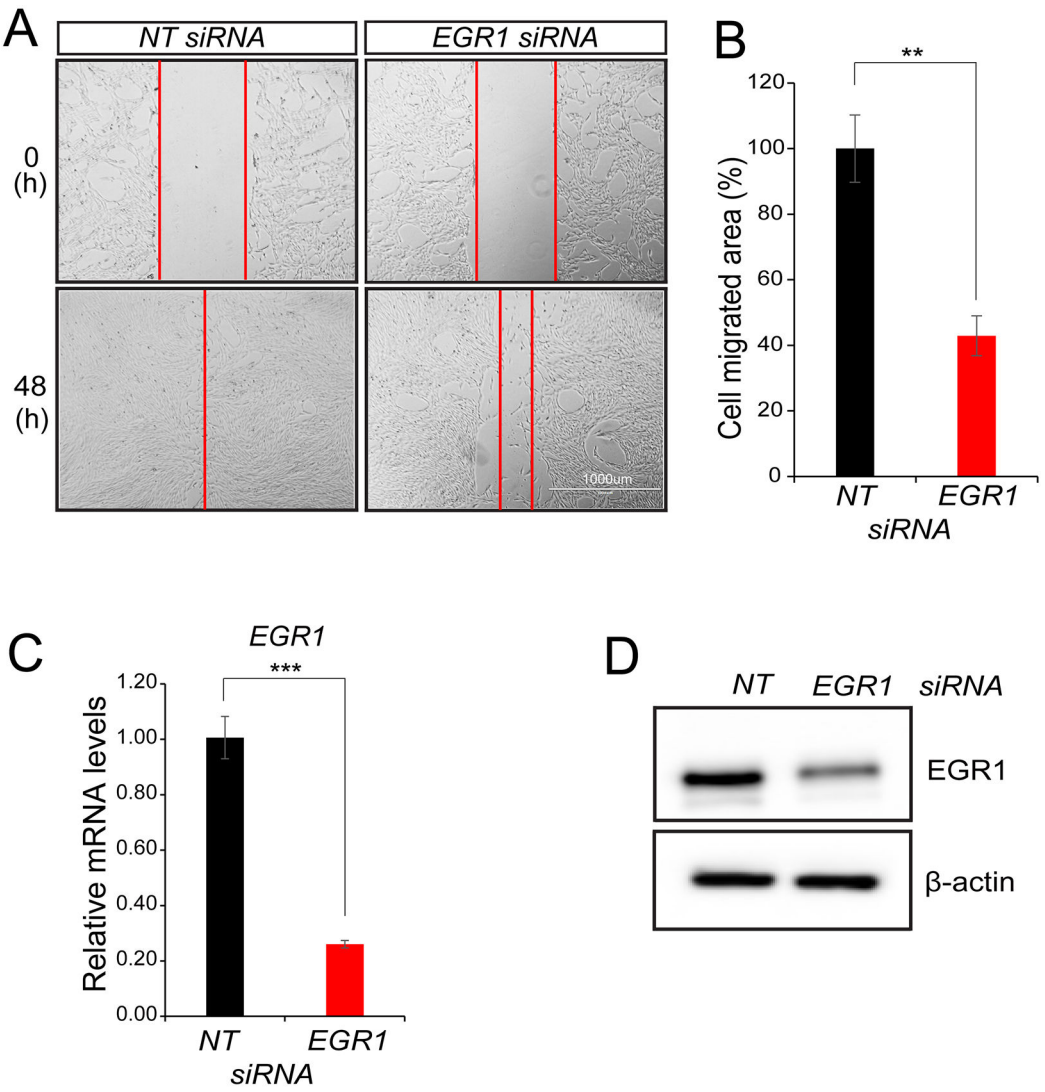

Figure 3.

EGR1 is required for iHEEC migration *in vitro*. (A) The migration ability of iHEEC was assessed by the wound healing assay. Representative bright-field images of the migrated area forty-eight hours following the scratch; scale bar applies to both images. (B) The histogram displays the reduced migration ability of iHEECs following EGR1 knockdown, specifically showing 60% reduced migration ability of iHEECs compared to control. (C-D) Both qPCR and Western immunoblot results confirm that EGR1 expression levels are significantly attenuated at the RNA and protein level respectively forty-eight hours following transfection with *NT* or *EGR1* siRNAs. For Western immunoblot analyses, β-actin served as a control for equal protein loading per lane. Results represent the mean ± SE and representative of three independent experiments; ** p-value<0.01; and *** p-value<0.001.

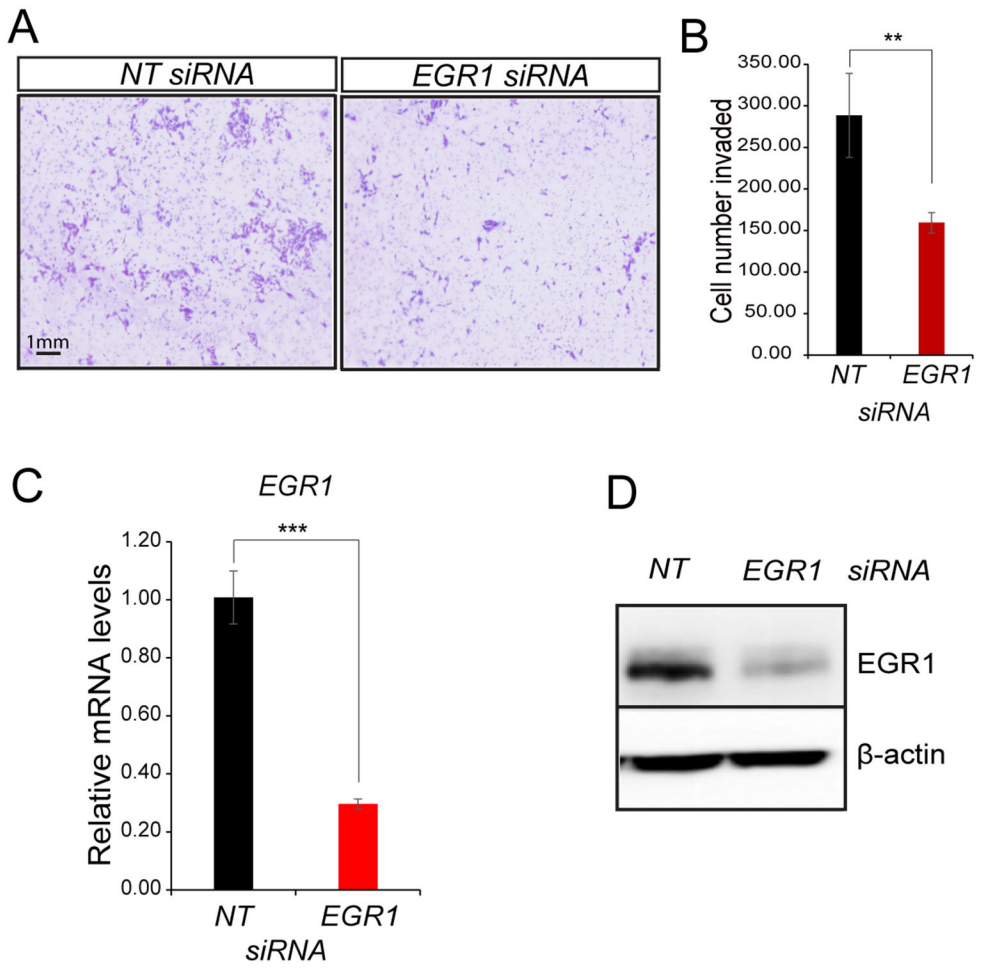

Figure 4.

Attenuation of EGR1 levels reduces the invasive capability of the iHEEC line *in vitro*. (A) Forty-eight hours following transfection with siRNAs targeting *NT* or *EGR1*, cell invasion analysis was initiated. Representative cell images are shown following the invasion experiment using either *NT* siRNA or *EGR1* siRNA transfected cells; the scale bar applies to all images. (B) Representative histogram quantitatively displays the number of *EGR1* siRNA transfected endometriotic epithelial cells that invaded the lower chamber compared with endometriotic epithelial cells transfected with *NT* siRNAs. (C-D) Both qPCR and Western immunoblot analyses confirm a significant reduction in EGR1 expression at the RNA and protein level respectively. Note: β-actin was used as a protein loading control. Results are represented as mean ± SE and representative of three independent experiments; ** p-value<0.01 and *** p-value<0.001.

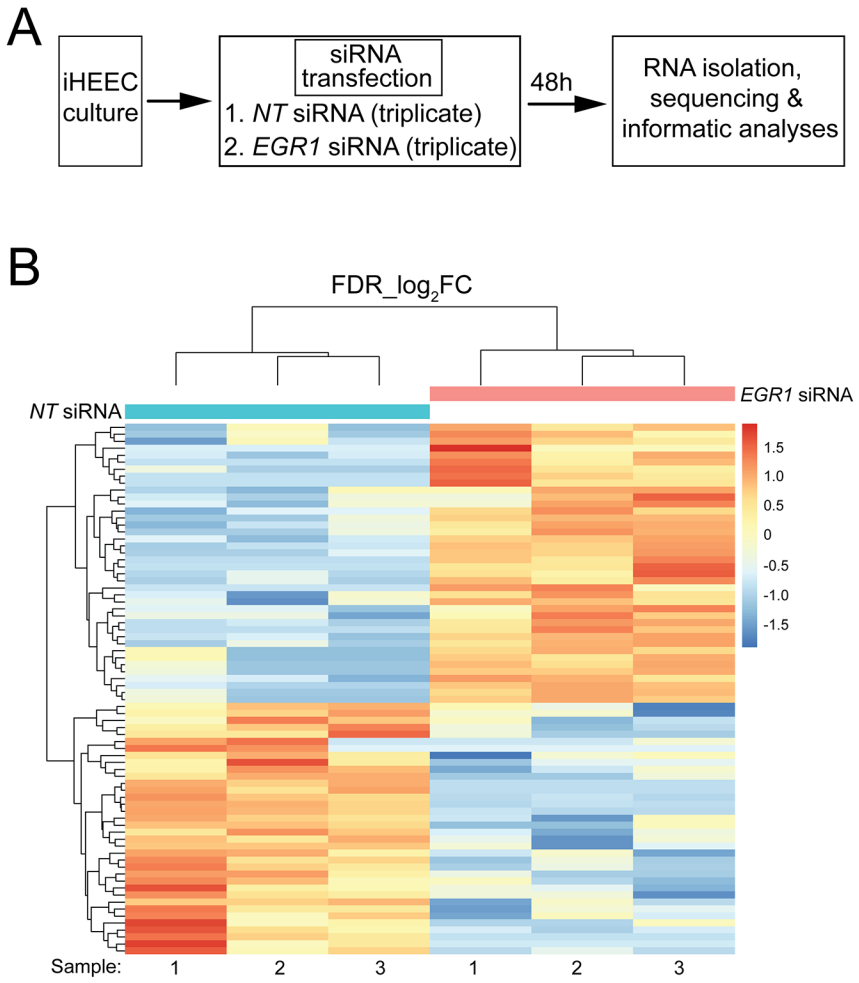

Figure 5.

Changes in the iHEEC transcriptome following EGR1 knockdown. (A) Experimental design of the RNA-seq experiment; triplicate samples were used for *NT* siRNA and *EGR1* siRNA groups. (B) Heatmap of clustering of genes with the same expression level differentially expressed (up or down) between the *NT* siRNA and *EGR1* siRNA groups. With a FDR<0.05 and a IFCI >1.5, 76 genes differentially expressed between *NT* siRNA and *EGR1* siRNA groups were clustered and presented as a heat map; each horizontal row represents a single gene. Warmer (*i.e.* reds) and cooler colors (*i.e.* blues) represent higher and lower expression respectively; the vertical color key on the right indicates the intensity with normalized expression values.

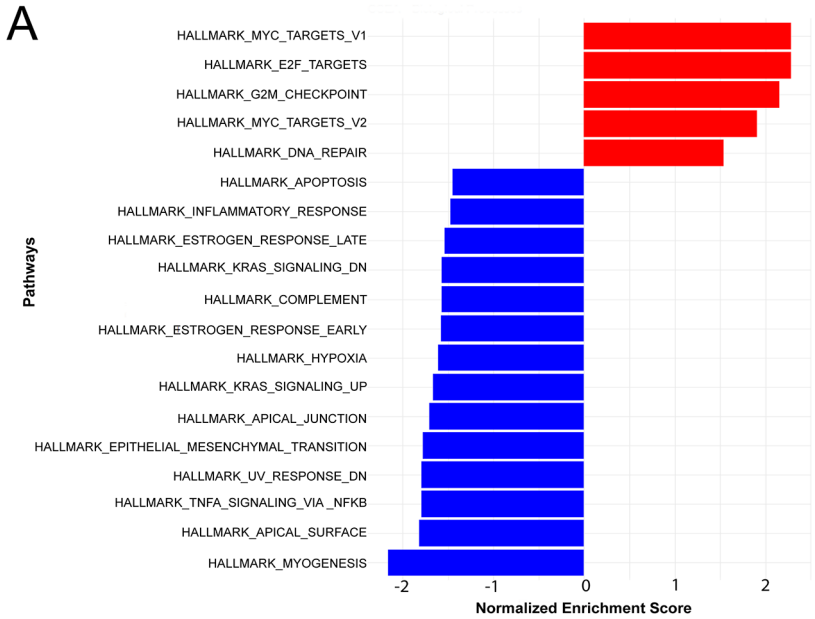

B

Annotation Cluster Term	Gene #	Enrichment Score
GO:0046888~negative regulation of hormone secretion	7	
GO:0005125~cytokine activity	15	
GO:0005126~cytokine receptor binding	13	
GO:0019221~cytokine-mediated signaling pathway	23	
GO:0071345~cellular response to cytokine stimulus	27	
GO:0006935~chemotaxis	20	
GO:0042330~taxis	20	
GO:0034097~response to cytokine	27	
GO:0005102~receptor binding	40	
GO:0042981~regulation of apoptotic process	38	
GO:0043067~regulation of programmed cell death	38	
GO:0010941~regulation of cell death	40	
GO:0042127~regulation of cell proliferation	41	
GO:0040011~locomotion	40	
GO:0002376~immune system process	63	
GO:0006955~immune response	39	
GO:0006915~apoptotic process	43	

0 2 4 6 8 10

Figure 6.

Pathway analyses of differential expressed genes in iHEECs following *EGR1* knockdown. (A) GSEA of differential expressed genes between the *NT* siRNA and *EGR1* siRNA groups showing normalized enrichment scores for listed Hallmark pathways. On the x-axis, normalized enrichment scores for gene expression changes (up or down represented by red and blue bars respectively) following a reduction in *EGR1* levels in iHEECs; the y-axis displays hallmark gene-sets representing well-defined biological states or processes (Liberzon et al., 2011). (B) DAVID gene functional clustering analysis of genes differentially expressed between the *NT* siRNA and *EGR1* siRNA treated iHEEC groups.

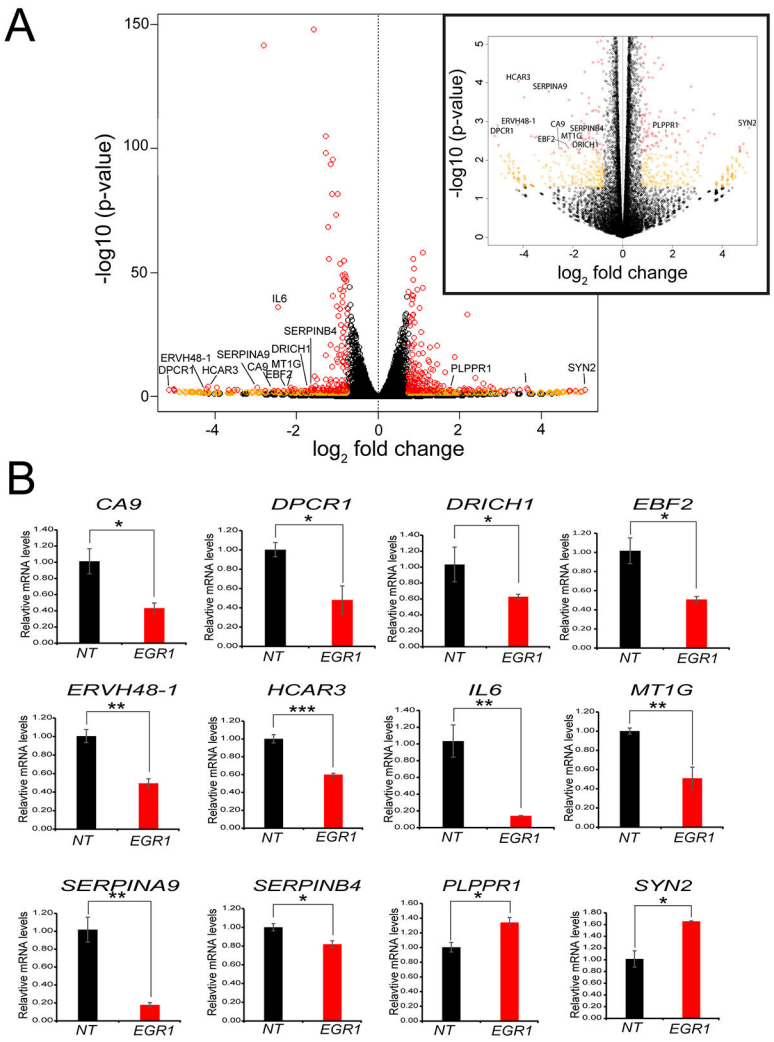

Figure 7.

Expression validation of a select number of genes for which expression levels change in response to *EGR1* knockdown in iHEECs. (A) Global gene expression changes displayed as a volcano plot represent the statistical significance (plotted as the log-transformed *p*-value) *versus* the fold change across all genes. To aid visualization, the insert on the right represents a magnification of the volcano plot of genes with a – log10 (*p*-value) up to 5. Individual genes are presented by open colored circles. Orange circles represent genes with an absolute fold change ≥ 1.5 and a *p*-value ≤ 0.05; red circles denote genes that also have an FDR ≤ 0.05. (B) Genes (10 downregulated and 2 upregulated following *EGR1* knockdown) annotated in (A) were validated by qPCR.

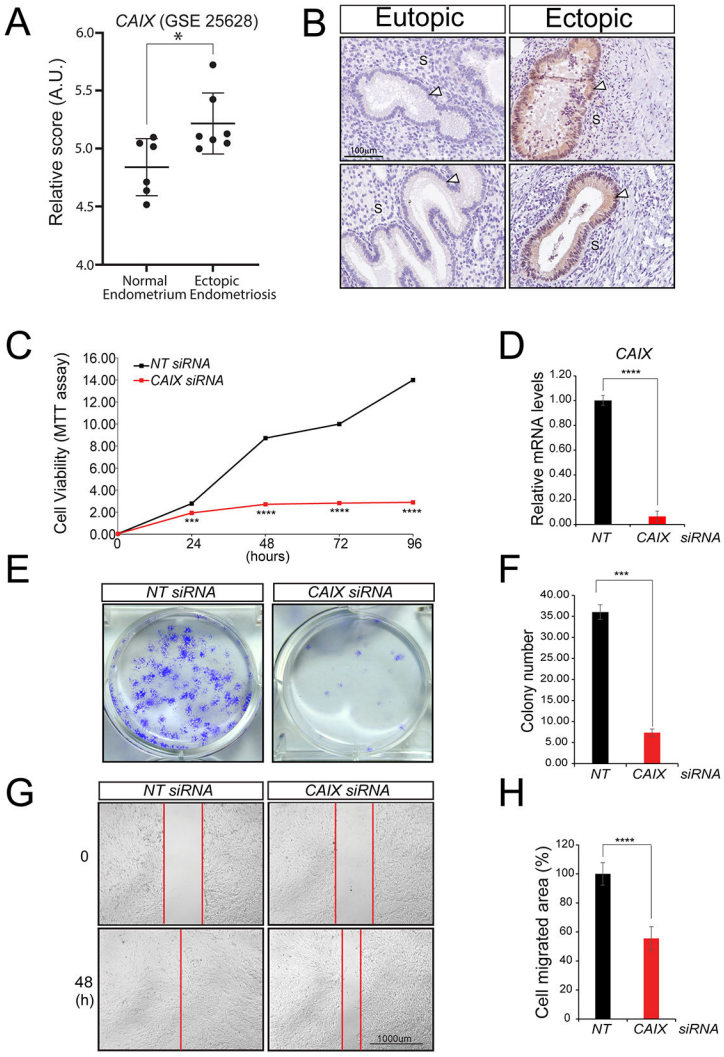

Figure 8.

Carbonic anhydrase IX is required to maintain the pathogenic properties of iHEECs. (A) The relative raw abundance of *CAIX* transcripts in human ectopic and matched control endometrium (from: Gene Expression Omnibus dataset GSE25628 (Crispi et al., 2013)). Note: *CAIX* transcripts are significantly elevated in human ectopic endometriosis compared with control endometrium (AU denotes arbitrary units). Human control and ectopic endometrial tissues were obtained during the proliferative phase. Data are presented as mean SE (control endometrium: n=6; ectopic endometrium: n=7); **p-value* ≤0.05. (B) Immunohistochemical analysis shows that CAIX is undetectable in the baboon eutopic endometrium (top and bottom left panels represent two separate baboon eutopic endometrial tissues). Ectopic endometriotic lesions (right panels (top and bottom)) express CAIX that is restricted to epithelial cells (white arrowhead); “S” indicates stromal compartment. The scale bar shown in left top panel applies to all four panels in (B). (C-H) Cell viability, clonogenic survival, and wound healing assays respectively show that *CAIX* depletion in iHEECs results in a compromised ability to proliferate, form colonies, and migrate—all pathogenic properties of iHEECs. Results are represented as mean ± SE

and representative of three independent experiments; *p-value<0.05, ***p-value<0.001 and ****p-value<0.0001.

Table 1

Human TaqMan expression assays

Gene	ID	Catalog number
CAIX	768	Hs00154208_m1
DRICH1	51233	Hs01589059_m1
DPCR1	135656	Hs00369879_m1
EBF2	64641	Hs00970588_m1
EGR1	1958	Hs00152928_m1
EGR2	1959	Hs00166165_m1
EGR3	1960	Hs04935588_m1
ERVH48-1	90625	Hs05577546_g1
HCAR3	8843	Hs02341102_s1
HTR3E	285242	Hs00704511_s1
IL6	3569	Hs00174131_m1
MT1G	4495	Hs04401199_s1
PLPPR1	54886	Hs00214827_m1
SERPINA9	327657	Hs00900935_m1
SERPINB4	6318	Hs01691258_g1
SYN2	6854	Hs00923900_m1
18S rRNA		4319413E

Table 2.

Top 35 downregulated genes with ≥ 1.5 log2FC and ≤ 0.05 FDR

GENE SYMBOL	GENE ID	GENE NAME	log2FC
DPCR1	135656	diffuse panbronchiolitis critical region 1	−5.13541
HPCA	3208	hippocalcin	−5.02329
LINC02043	102724699	long intergenic non-protein coding RNA 2043	−5.00908
SFTPA2	729238	surfactant protein A2	−4.98471
ERVH48-1	90625	endogenous retrovirus group 48 member 1	−4.20807
HCAR3	8843	hydroxycarboxylic acid receptor 3	−4.18165
LINC00302	388699	long intergenic non-protein coding RNA 302	−3.96066
MIR4531	100616355	microRNA 4531	−3.66491
PPIAL4G	644591	peptidylprolyl isomerase A like 4G	−3.52393
MIR2116	100313886	microRNA 2116	−3.44583
SERPINA9	327657	serpin family A member 9	−2.96628
EGR1	1958	early growth response 1	−2.80233
MIR6071	102466516	microRNA 6071	−2.76669
CA9	768	carbonic anhydrase 9	−2.5501
IGBP1P1	280655	immunoglobulin (CD79A) binding protein 1 pseudogene 1	−2.45972
IL6	3569	interleukin 6	−2.44627
WARS2-IT1	104472716	WARS2 intronic transcript 1	−2.32034
EBF2	64641	early B-cell factor 2	−2.18673
SNORA69	26779	small nucleolar RNA, H/ACA box 69	−2.14905
MT1G	4495	metallothionein 1G	−2.13078
TOMM20L	387990	translocase of outer mitochondrial membrane 20 like	−2.06042
GOLGA2P7	388152	golgin A2 pseudogene 7	−2.03929
LINC02056	102477328	long intergenic non-protein coding RNA 2056	−1.88876
LINC01364	100505768	long intergenic non-protein coding RNA 1364	−1.81405
DRICH1	51233	aspartate rich 1	−1.77817
SNORD55	26811	small nucleolar RNA, C/D box 55	−1.72796
CHRNA3	1136	cholinergic receptor nicotinic alpha 3 subunit	−1.66121
ZNF804A	91752	zinc finger protein 804A	−1.63954
SERPINB4	6318	serpin family B member 4	−1.63168
SCOC-AS1	100129858	SCOC antisense RNA 1	−1.61592
CERCAM	51148	cerebral endothelial cell adhesion molecule	−1.57345
ARTN	9048	artemin	−1.56061
TAGLN3	29114	transgelin 3	−1.55785
JPH1	56704	junctophilin 1	−1.54813
MYO16	23026	myosin XVI	−1.52762

Table 3.

Top 35 upregulated genes with ≥ 1.5 log2FC and ≤ 0.05 FDR

GENE SYMBOL	GENE ID	GENE NAME	log2FC
SYN2	6854	synapsin II	5.082034
MIR579	693164	microRNA 579	4.987176
CFAP99	402160	cilia and flagella associated protein 99	4.84547
AGBL4	84871	ATP/GTP binding protein like 4	4.717173
ALLC	55821	allantoicase	4.706209
LINC02324	100128233	long intergenic non-protein coding RNA 2324	4.702674
MIR7112	102465906	microRNA 7112	4.700377
HTR3E	285242	5-hydroxytryptamine receptor 3E	4.693637
TCERG1L	256536	transcription elongation regulator 1 like	3.674137
ADAMTSL2	9719	ADAMTS like 2	3.656694
TJP3	27134	tight junction protein 3	3.483605
MAGI1-AS1	100873983	MAGI1 antisense RNA 1	3.321479
TEC	7006	tec protein tyrosine kinase	3.218295
SPN	6693	sialophorin	3.124289
FAM213A	84293	family with sequence similarity 213 member A	3.017358
TDGF1	6997	teratocarcinoma-derived growth factor 1	2.81775
CCDC102B	79839	coiled-coil domain containing 102B	2.622383
HMMR-AS1	101927813	HMMR antisense RNA 1	2.587966
ZFX-AS1	100873922	ZFX antisense RNA 1	2.486735
LRMP	4033	lymphoid restricted membrane protein	2.459547
TSPAN2	10100	tetraspanin 2	2.38303
HOXA6	3203	homeobox A6	2.30578
HR	55806	hair growth associated	2.263117
CXCL10	3627	C-X-C motif chemokine ligand 10	2.237354
SCG2	7857	secretogranin II	2.187924
TEKT2	27285	tektin 2	2.183893
SYTL5	94122	synaptotagmin like 5	2.120299
TIGIT	201633	T-cell immunoreceptor with Ig and ITIM domains	2.11793
RCAN2	10231	regulator of calcineurin 2	1.884025
PLPPR1	54886	phospholipid phosphatase related 1	1.781885
TEX14	56155	testis expressed 14, intercellular bridge forming factor	1.761584
FAM84B	157638	LRAT domain containing 2	1.735547
TNFSF10	8743	TNF superfamily member 10	1.653359
CPA4	51200	carboxypeptidase A4	1.604515
MAP3K14-AS1	100133991	MAP3K14 antisense RNA 1	1.543323